Journal of Applied Polymer Science

# Preparation and characterization of antimicrobial PVA hybrid films with *N*-halamine modified chitosan nanospheres

**Maoli Yin,[1] Xiaoli Chen,[1] Rong Li,[1] Dan Huang,[1] Xiaoyan Fan,[1] Xuehong Ren,[1] Tung-Shi Huang[2]**

[1]Key Laboratory of Eco-Textiles of Ministry of Education, Jiangsu Engineering Technology Research Center for Functional Textiles, College of Textiles and Clothing, Jiangnan University, Wuxi, Jiangsu 214122, China

[2]Department of Poultry Science, Auburn University, Auburn, Alabama 36849

Correspondence to: X. Ren (E-mail: xhren@jiangnan.edu.cn)

**ABSTRACT:** Chitosan is a promising candidate as an antimicrobial agent in food packaging materials and biomaterials due to its biocompatibility, biodegradability, non-toxicity and biocidal activity. In this study, chitosan derivatives, α-(5,5-dimethyl hydantoin amino)-chitosan (CS-HDH), were synthesized. The CS-HDH nanospheres were prepared by ionic gelation method and characterized by SEM, FT-IR, XRD, and TGA-DTG. The prepared novel chitosan nanospheres in the range of 200–300 nm had good dispersibility. The CS-HDH nanospheres were used to prepare antibacterial PVA hybrid films by solvent evaporation technique. The surface morphology and thermal property of hybrid films were measured by SEM, AFM, and TGA-DTG. The results of antibacterial test showed that the hybrid film with $1.24 \times 10^{18}$ atoms/cm$^2$ of active chlorine exhibited excellent antibacterial properties against *Staphylococcus aureus* and *Escherichia coli* O157:H7, and all of bacteria could be inactivated within 5 min. © 2016 Wiley Periodicals, Inc. J. Appl. Polym. Sci. **2016**, *133*, 44204.

**KEYWORDS:** biomaterials; composites; films

Received 6 April 2016; accepted 18 July 2016
**DOI: 10.1002/app.44204**

## INTRODUCTION

To prevent the growth of microorganisms, the application of antibacterial materials in food packaging has attracted much attention over the past few years.[1,2] A variety of antibacterial compounds such as inorganic nano-antibacterial agents,[3] *N*-halamines,[4] quaternary ammonium salts,[5] chitosan,[6] and some natural materials,[7,8] have been developed as potential antimicrobial components in packaging materials.

Chitosan is a natural polymer composed of glucosamine and a small amount of *N*-acetyl glucosamine through β-1,4-glycosidic bond. As a polycationic natural polymer, chitosan has a broad spectrum of antibacterial properties because it contains many easily protonated amino groups. In addition, chitosan is nontoxic, has good biocompatibility, and is biodegradable making it feasible to apply in films for an antimicrobial purpose, although its antimicrobial property is moderate under acidic condition. In recent years, there has been a growing interest in introducing functional molecular substituents with chitosan by chemical modification including quaternization, carboxylation, and acylation improving the physical and chemical properties and extending its application.[9–11] Research in nano-structural chitosan has great potential in the preparation of antibacterial materials due to its unique property of large surface area to volume ratio. Ali *et al.* synthesized silver loaded chitosan nanoparticles with average particle size of 165 nm by ionic gelation with sodium tripolyphosphate (TPP) and silver ions.[12] Pan *et al.* developed pH responsive-chitosan nanoparticles through two-step crosslinking method to control the release of protein drug.[13]

*N*-halamine materials have been extensively explored over the past few decades due to their fast inactivation of a broad spectrum of microorganisms.[14,15] The antibacterial mechanism of *N*-halamine is directly affected by the surface area of the materials and plays an important role in antibacterial efficacy.[16] The higher surface area provides more contact sites with bacteria, which increase inactivation rate. Dong *et al.* synthesized *N*-halamine-functionalized silica nanoparticles which showed 2-8 times higher antibacterial activity than the bulk counterparts.[17]

*N*-halamine chitosan derivative has been synthesized by the incorporation of *N*-halamine compound in chitosan to enhance its antibacterial efficacy.[18] In this study, novel nanospheres of *N*-halamine modified chitosan derivative were prepared with TPP by ionically cross-linking. The method used in this study not only overcame the antibacterial activity dependency of chitosan on pH, it also enhanced the antibacterial efficiency comparing with other modification methods.[12,19] The synthesized *N*-halamine modified chitosan nanospheres were blended with poly(vinyl alcohol) (PVA) to

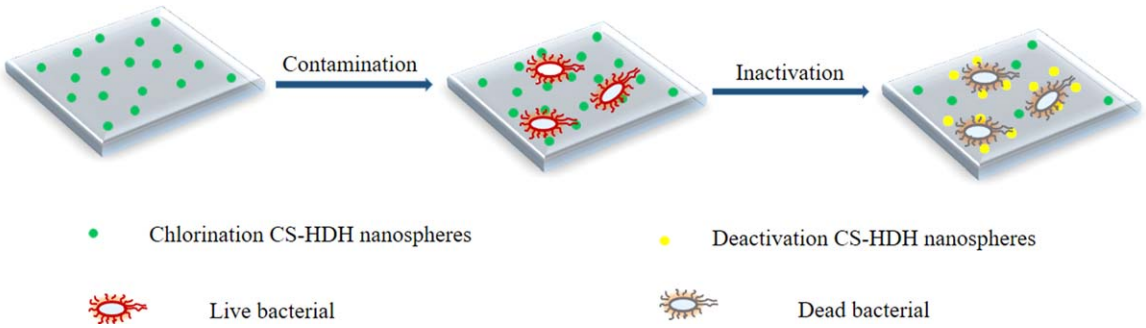


**Figure 1.** Schematic illustration of the inactivation process of hybrid film. [Color figure can be viewed in the online issue, which is available at wileyonlinelibrary.com.]

prepare antibacterial hybrid films (Figure 1). The antibacterial properties of the hybrid films against *Staphylococcus aureus* and *Escherichia coli* O157:H7 were evaluated. In addition, the mechanical properties and thermal properties of films were investigated. This study aims to prepare novel antibacterial chitosan nanospheres which were blended with PVA to produce food packaging or biomaterials films with excellent antibacterial properties.

## EXPERIMENTAL

### Materials and Reagents

Chitosan (average molecular weight of 50 kDa, 90% deacetylation) was purchased from Zhejiang Aoxing Biochemical, China. 1-Hydroxymethyl-5,5-dimethylhydantoin (HDH) was obtained from TCI, Shanghai, China. Glacial acetic acid (analytical grade), acetone (purity > 99.5%), sodium TPP, household bleach, and PVA were purchased from Sinopharm Chemical Reagent (Shanghai, China). All reagents were used as received without further purification. The bacteria used were *S. aureus* (ATCC 6538) and *E. coli* O157:H7 (ATCC 43895) (American Type Culture Collection, Rockville, MD). The trypticase soy agar (TSA) was from Difco Laboratories, Detroit, MI.

### Instruments

Measurement of particle size and polydispersity (size distribution) of the CS-HDH nanospheres suspension was performed using a Zeta Potential Analyzer (Brookhaven Instruments Corporation, TX). The FT-IR spectra of chitosan, CS-HDH and CS-HDH nanospheres and hybrid films were recorded by a NICOLET are 10 in the optical range of 500–4000 $cm^{-1}$ by averaging 16 scans at a resolution of 4 $cm^{-1}$. X-ray patterns of CS-HDH, CS-HDH nanospheres were obtained by a D8 Advance X-ray diffraction. Thermogravimetric analysis (TGA) was carried out using a TGA unit (NETZSCH STA 499 F3). The SEM images and AFM photograph were obtained from SU-1510 scanning electron microscope (Hitachi,Tokyo, Japan) and CSPM-3000 atomic force microscope, respectively. The mechanical properties of film were determined according to ASTM D3039 methodology in a computer controlled electronic universal testing machine (3385H).

### Preparation of Antibacterial Hybrid Film

**Modification of Chitosan with HDH.** CS-HDH (Figure 2) was prepared according to previous literature.[18] Chitosan with 3.22 g (0.05 mol) was dissolved in 1% (v/v) glacial acetic acid solution. Then, 3.16 g (0.05 mol) of HDH were added into the solution and stirred at 100 °C for 24 h. After the reaction, water was removed under vacuum followed by adding excess acetone. The precipitate was filtered and washed thoroughly with acetone, and dried in a vacuum oven at 55 °C for 48 h. The solid powder was weighed for calculating grafting ratio.

**Synthesis of CS-HDH Nanospheres.** CS-HDH nanospheres (Figure 3) were formed by ionically cross-linking through protonated residual amino groups and TPP phosphate anions.[19] CS-HDH was dissolved in 1% (v/v) glacial acetic acid solution. CS-HDH concentration was at 4.0 mg/mL with pH 6.0. TPP solutions at 2.0 mg/mL which were added drop by drop to the CS-HDH solutions (volume ratio of TPP to CS-HDH is 1:5) under magnetic stirring. The mixed solution was stirred for 60 min at room temperature to produce nanospheres suspensions.

**Chlorination CS-HDH Nanospheres.** CS-HDH nanosphere suspensions were soaked in 5% solution of household bleach at pH 7 (adjusted with 1N $H_2SO_4$) with stirring at ambient temperature for 2 h. After chlorination, samples were centrifuged and washed thoroughly with distilled water to remove free chlorines. The resulted solid powder was dried at 50 °C for 12 h to remove any unbounded chlorines from the nanospheres.

**Preparation of CS-HDH Nanospheres/PVA Hybrid Film.** Five percent of PVA was completely dissolved in deionized water at 90 °C. After the PVA solution cooled down to room temperature, different percents volumes of the chlorinated CS-HDH nanospheres were added to the PVA solutions to make mass ratios of the chlorinated CS-HDH nanospheres to PVA at 5, 10, 15, and 20%. The mixture was stirred for 1 h to obtain a uniform blending solution and poured into a teflon mold. Then, the sample was dried in an oven at 45 °C for 1 h to obtain the desired hybrid film.

### Chlorine Analytical Titration

The chlorine content of the samples was determined by the iodometric/thiosulfate titration procedure. Hybrid films (2 cm

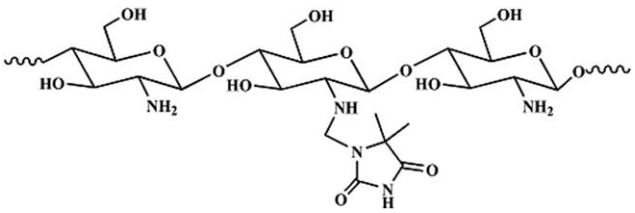


**Figure 2.** The structure of CS-HDH.

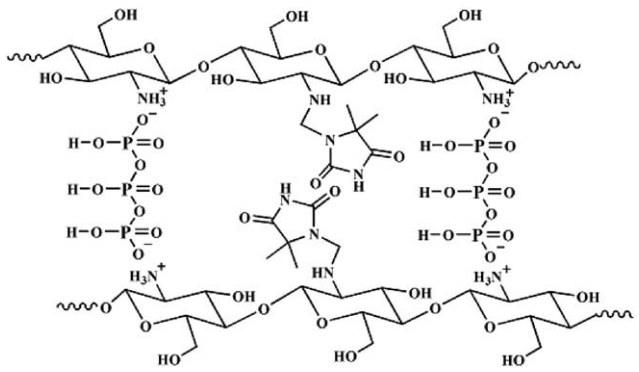

**Figure 3.** Schematic diagram of ionic cross-linking between CS-HDH and TPP.

× 2 cm) were put in a 50 mL beaker containing 20 mL of deionized water. Then, 0.5 g of KI and a few drops of 1% of starch solution were added. After stirring for a while, the solution was titrated with 0.001 N sodium thiosulfate. The chlorine loadings of the hybrid films were calculated with the following equation:

$$Cl^{+}(atom/cm^{2}) = \frac{N \times V \times 6.023 \times 10^{23}}{2 \times S}$$

where, $N$ and $V$ are the normality (equiv/L) and volume (L) of the titrant sodium thiosulfate, respectively, and $S$ is the area of the films in $cm^2$.

### Antibacterial Test

The biocidal efficacies of hybrid films were evaluated against *S. aureus* (ATCC 6538) and *E. coli* O157:H7 (ATCC 43895) using a modified AATCC Test Method 100-2004. The test began with the addition of 25 μL of the bacterial suspensions to the center of a 2.54 cm square hybrid film, and then, the suspension was covered with another identical hybrid film and topped with a weight. After contact times of 5, 10, 30, and 60 min, the films were quenched with 5.0 mL of sterile 0.02 N sodium thiosulfate solution and vortexed to remove all oxidative chlorine. The quenched solutions were diluted, and plated on TSA plates. The plates were incubated at 37 °C for 24 h. The bacterial colonies were recorded and enumerated for biocidal efficacy analysis.

## RESULTS AND DISCUSSION

### Characterization of CS-HDH Nanospheres by SEM, FT-IR, and XRD

The nanospheres were prepared with 4.0 mg/mL CS-HDH and 2.0 mg/mL TPP (volume ratio of TPP to CS-HDH is 1:5). The morphological characteristics of the CS-HDH nanospheres were examined by SEM. Figure 4(A) shows that the CS-HDH nanospheres have a size of about 300 nm which was further conformed by Zeta Potential Analyzer, and are dispersed well without significant accumulation. Figure 4(B) shows the CS-HDH nanospheres have irregular shape with clear boundaries.

The FT-IR spectra of CS, CS-HDH, and CS-HDH nanospheres (NPS) are shown in Figure 5. The characteristic absorption band of chitosan at 1597 $cm^{-1}$ is due to the amide II bending vibration. Compared with chitosan, the intensity of amine bending vibration at 1597 $cm^{-1}$ decreased in CS-HDH's FT-IR spectra due to the new absorption peak of the secondary amino group at 1654 $cm^{-1}$. The carbonyl absorption peak at 1705 $cm^{-1}$ is attributed to the presence of hydantoin ring. FT-IR spectra of CS-HDH nanospheres showed that the vibration band of C═O shifted to 1715 $cm^{-1}$ due to the inductive effect of N─Cl. It can be found that two new peaks appeared at 1627 $cm^{-1}$ and 1244 $cm^{-1}$ respectively, which are assigned to antisymmetric deformation vibration of N-H due to the presence of $NH_3^+$ groups and $PO_2^-$ groups. These bands were not observed for CS and CS-HDH, which confirmed that CS-HDH nanospheres were produced by CS-HDH and TPP through ionic crosslinking.[20]

Crystallographic structures of chitosan, CS-HDH, and CS-HDH nanospheres were determined by X-ray diffraction and presented in Figure 6. There is a stronger peak at 19.87° and a relatively weaker peak at 10.48° in the diffractogram of chitosan, which indicated the presence of two different crystal structures belonged to monoclinic system with high degree of chitosan crystallinity. The peak at 10.48° disappeared in the XRD pattern of CS-HDH, and the peak at 19.87° became weaker and wider, which indicates that CS-HDH has lower degree of crystallinity than chitosan. However, no peak was found in the diffractogram of CS-HDH nanospheres, which displays greater disarray in chain alignment in the nanospheres after crosslinking. CS-HDH nanospheres consisted of a dense network structure of interpenetrating polymer chains crosslinked by TPP counter ions.[12]

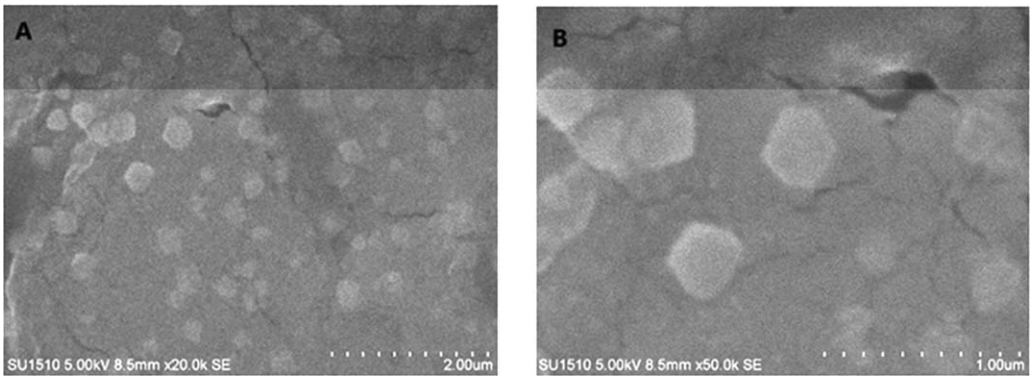


**Figure 4.** SEM micrograph of CS-HDH nanospheres. (A) 20.0 k magnification and (B) 50.0 k magnification.

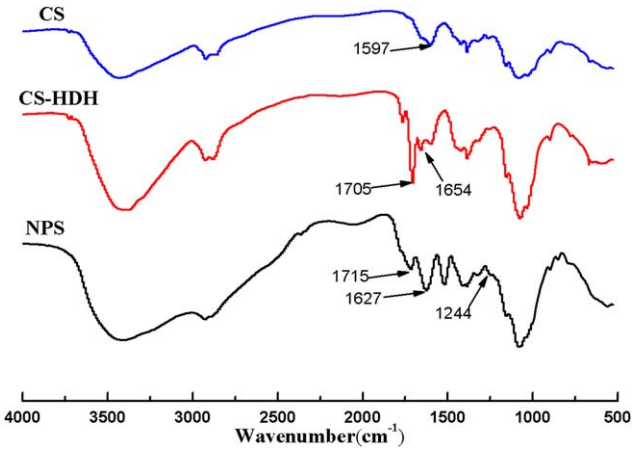


**Figure 5.** The FT-IR spectra of chitosan, CS-HDH, and CS-HDH nanospheres. [Color figure can be viewed in the online issue, which is available at wileyonlinelibrary.com.]

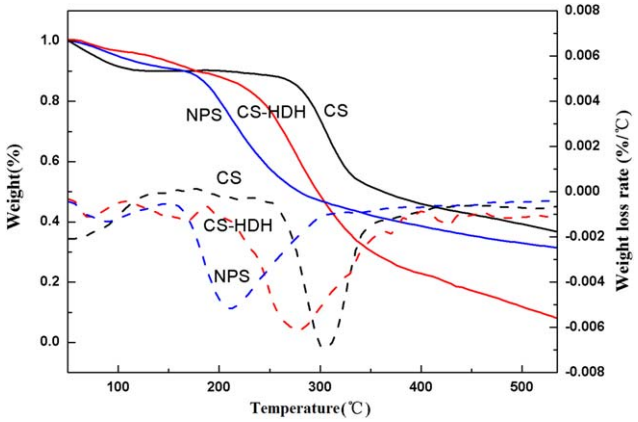


**Figure 7.** The TGA and DTG curves for chitosan, CS-HDH, and CS-HDH nanospheres. [Color figure can be viewed in the online issue, which is available at wileyonlinelibrary.com.]

### Thermal Properties of CS-HDH Nanospheres

TGA-DTG of chitosan, CS-HDH, and CS-HDH nanospheres showed two stages of weight loss (Figure 7). The first stage weight loss may be due to the loss of adsorbed and bound water, and the second stage weight loss is due to the thermal degradation. The first stage weight loss of chitosan is about 10% from 50 to 135 °C, and the second stage weight loss is about 40% from 260 to 345 °C. For CS-HDH, the first stage weight loss is approximately 14% from 50 to 200 °C, and the second phase weight loss is 58% from 225 to 370 °C. CS-HDH has higher weight loss of moisture and thermal degradation than chitosan because HDH could destroy hydrogen bonds, reduce the degree of crystallinity, and form more amorphous regions. In addition, the thermal decomposition of CS-HDH started at earlier onset temperature and had wider range. For CS-HDH nanospheres, the degradation behavior is somewhat similar to chitosan. The initial stage of weight loss is 10% from 50 to 155 °C, and the second stage weight loss is about 43% from 170 to 300 °C. CS-HDH nanospheres showed better thermal stability than CS-HDH due to the existence of inorganic phosphorous in the nanospheres.[12]

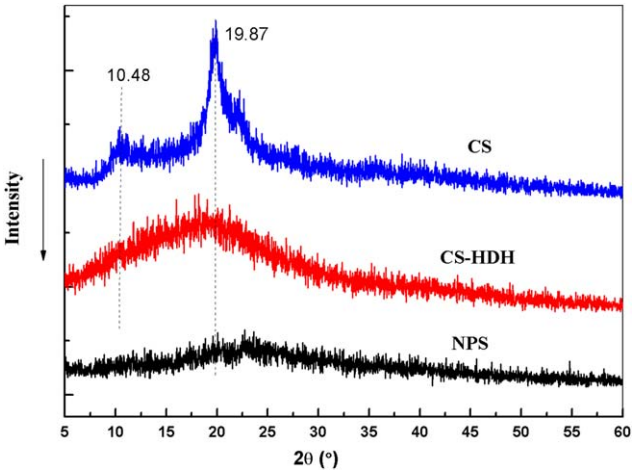


**Figure 6.** XRD patterns of chitosan, CS-HDH, and CS-HDH nanospheres. [Color figure can be viewed in the online issue, which is available at wileyonlinelibrary.com.]

### The Chlorine Content and Mechanical Properties of Hybrid Film

Generally, the higher chlorine content of *N*-halamine antibacterial materials provides higher inactivation rate as more N-Cl bonds on the surface can contact with microbes leading to quicker inactivation. Table I shows the chlorine contents of hybrid films with different mass ratios of CS-HDH nanospheres to PVA. The chlorine content of hybrid films was enhanced with the increase of the mass ratio of CS-HDH nanospheres to PVA. The chlorine content increased from $1.92 \times 10^{17}$ atoms/cm$^2$ to $1.24 \times 10^{18}$ atoms/cm$^2$ when the mass ratio of CS-HDH nanospheres to PVA increased from 5% to 15%. CS-HDH nanospheres/PVA hybrid film with chlorine over $1.00 \times 10^{18}$ atoms/cm$^2$ was used for further testing.

**Table I.** Effect of CS-HDH nanospheres to PVA mass ratio on chlorine content

| CS-HDH nanospheres to PVA mass ratio (%) | Chlorine content of per unit area (atom/cm$^2$) |
|---|---|
| 0 | — |
| 5 | $1.92(\pm0.23) \times 10^{17}$ |
| 10 | $7.11(\pm0.56) \times 10^{17}$ |
| 15 | $1.24(\pm0.17) \times 10^{18}$ |
| 20 | $1.69(\pm0.24) \times 10^{18}$ |

**Table II.** Mechanical properties of the PVA and hybrid films

| Samples | Tensile strength (MPa) | Percentage elongation (%) | Young's modulus (MPa) |
|---|---|---|---|
| PVA film | 19.05 ± 1.70 | 266.3 ± 5.87 | 125.14 ± 4.12 |
| Hybrid film | 17.36 ± 1.32 | 215.6 ± 2.8 | 65.43 ± 3.30 |

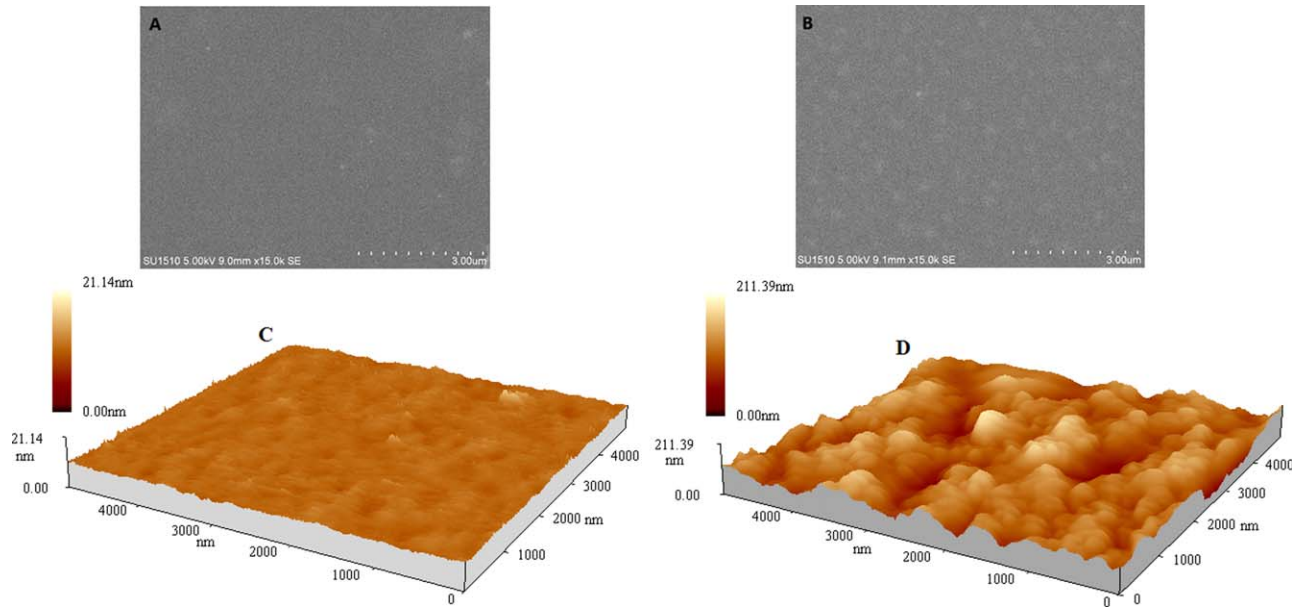


**Figure 8.** The SEM images and AFM photographs of (A,C) PVA film and (B,D) hybrid film. [Color figure can be viewed in the online issue, which is available at wileyonlinelibrary.com.]

The mechanical properties of the PVA and hybrid films were evaluated by tensile test and the results were shown in Table II. Compared with the PVA film, the tensile strength and elongation percentage of hybrid film decreased about 8.87% and 19.04%, respectively. However, the Young's modulus had a significant decrease from 125.41 to 65.43 MPa. The mechanical properties of film depended on the intermolecular forces, moisture content, the characteristic of the polymers used for blending, and the processing conditions.[21–23] The CS-HDH nanospheres as a additive may partly damage the ordered structure of PVA film and restrict the molecular chain segments motion, which were crucial to the tensile strength and elongation percentage.[23] The values for Young's modulus show that hybrid film could be easily deformed and was softer than PVA film.

### Surface Morphology of Hydrid Film by SEM and AFM

Figure 8(A,B) showed the SEM micrographs of PVA and hybrid films. The surface of PVA film is very smooth [Figure 8(A)]. While the surface image of the hybrid film [Figure 8(B)] showed dispersed particles embedded inside the film. The particle size of nanospheres is less than 300 nm which is similar to the value of CS-HDH nanospheres measured by Zeta Potential Analyzer. It can be found that nanospheres are uniformly distributed in the hybrid film, and there is no obvious phase separation. The PVA and hybrid films show different surface morphologies by AFM [Figure 8(C,D)]. Compared with PVA film, the hybrid film exhibits higher roughness parameters. The morphology of hybrid film is dependent on many factors including polymer solubility, particle size of nanospheres, solvent evaporation, phase separation, vitrification, total thickness, and surface composition.[24,25]

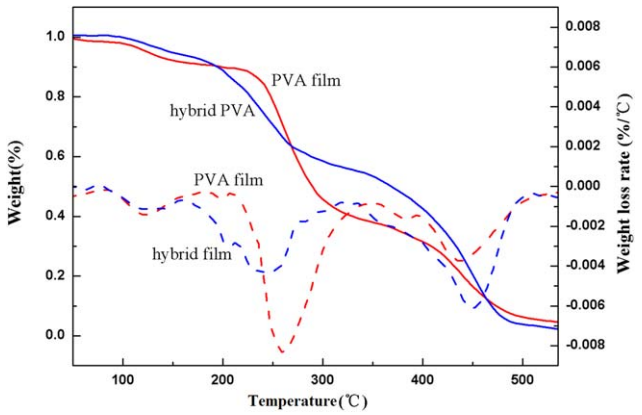


**Figure 9.** The TGA-DTG curves of PVA and hybrid films. [Color figure can be viewed in the online issue, which is available at wileyonlinelibrary.com.]

### Thermal Analysis of Hydrid Film

TGA-DTG curves of PVA and hybrid films are shown in Figure 9. There are three consecutive steps of weight loss in the curves. The weight loss of the first region at temperature 80–150 °C was about 10%, which was due to the loss of the adsorbed water and bound water.[26–28] The weight loss of PVA film in the second stage loss was about 50% at 220–320 °C, which corresponded to the rupture and decomposition of volatile products and dehydroxylation of the PVA.[27] In contrast, the weight loss of the hybrid film in the second stage was about 30% starting from 180 to 280 °C, which was caused by the formation of a non-unitary structure with the CS-HDH nanopheres, and the breaking of hydrogen bonds of PVA molecular chains and crystallinity.[28] Conversely, CS-HDH nanospheres containing phosphorus could reduce the rate of heat loss. The third weight loss region of PVA film started at 350 °C due to the combustion of the carbonaceous backbone.[28] The third weight loss region of the hybrid film showed a broader range and bigger weight loss, which is due to partial

**Table III.** Antibacterial property against *S. aureus*[a] and *E. coli* O157:H7[b]

| Samples | Contact Time (min) | *S. aureus*[a] | | *E. coli* O157:H7[b] | |
|---|---|---|---|---|---|
| | | % Reduction | Log reduction | % Reduction | Log reduction |
| PVA film | 60 | 17.59 | 0.08 | 14.36 | 0.07 |
| Hybrid film | 5 | 100 | 6.27 | 100 | 6.12 |
| | 10 | 100 | 6.27 | 100 | 6.12 |
| ($1.24 \times 10^{18}$ atoms/cm$^2$ $Cl^+$) | 30 | 100 | 6.27 | 100 | 6.12 |
| | 60 | 100 | 6.27 | 100 | 6.12 |

[a] Inoculum population was $1.87 \times 10^6$ CFU/swatch.
[b] Inoculum population was $1.33 \times 10^6$ CFU/swatch.

decomposition of main chain and the combustion of the carbonaceous backbone.[29]

**Antibacterial Efficacy**

The antibacterial efficacy results of PVA film and CS-HDH nanospheres/PVA hybrid film against Gram-positive *S. aureus* and Gram-negative *E. coli* O157:H7 at populations of about $10^6$ CFU/swatch are shown in Table III. The control PVA film provided a small degree of bacterial reduction (17.59% reduction of *S. aureus* and 14.36% reduction of *E. coli* O157:H7) with 60 min of contact, which was mainly caused by the adhesion of bacteria on the film. The hybrid film containing $1.24 \times 10^{18}$ atoms/cm$^2$ of active chlorine could inactivate 100% of *S. aureus* and *E. coli* O157:H7 with log reductions of 6.27 and 6.12 within 5 min of contact time, respectively. The antimicrobial results revealed that the CS-HDH nanospheres/PVA hybrid film has excellent antimicrobial activity compared with chitosan-GH film in a previous study.[30]

## CONCLUSIONS

In summary, CS-HDH nanospheres from the *N*-halamine modified chitosan derivative were synthesized using grafting and ionic gelation method. The synthesized CS-HDH nanospheres were blended with PVA to prepare antibacterial hybrid films. The hybrid films with *N*-halamine modified chitosan could enhance the antibacterial efficiency. The thermal analysis results showed that the thermal stability of CS-HDH nanospheres were better than that of CS-HDH. The antibacterial hybrid film containing $1.24 \times 10^{18}$ atoms/cm$^2$ of active chlorine exhibited excellent antimicrobial efficacies by inactivating six logs of *S. aureus* and *E. coli* O157:H7 within 5 min. CS-HDH nanospheres can not only enhance the antimicrobial properties of PVA film, it also improves their thermal stability. In addition, the tensile test results show that the hybrid film maintained relatively good mechanical strength. The prepared films are expected to apply in food packaging and biomaterials.

## ACKNOWLEDGMENTS

This work was supported by the Project of Jiangsu Science and Technological Innovation Team, the Science and Technology Department of Jiangsu Province of China (BY2014023-09), and the Scientific Research Foundation for Returned Overseas Chinese Scholars, Ministry of Education, China.

## REFERENCES

1. Cruz-Romero, M. C.; Murphy, T.; Morris, M.; Cummins, E.; Kerry, J. P. *Food Control* **2013**, *34*, 393.
2. Lavoine, N.; Givord, C.; Tabary, N.; Desloges, I.; Martel, B.; Bras, J. *Innov. Food Sci. Emerg. Technol.* **2014**, *26*, 330.
3. Dastjerdi, R.; Montazer, M. *Colloids Surf. B* **2010**, *79*, 5.
4. Ren, X.; Kocer, H. B.; Worley, S. D.; Broughton, R. M.; Huang, T. S. *Carbohydr. Polym.* **2009**, *75*, 683.
5. Buffet-Bataillon, S.; Tattevin, P.; Bonnaure-Mallet, M.; Jolivet-Gougeon, A. *Int. J. Antimicrob. Agents* **2012**, *39*, 381.
6. Chandrasekar, S.; Vijayakumar, S.; Rajendran, R. *Int. J. Antimicrob. Agents* **2014**, *4*, 59.
7. Morelli, C. L.; Mahrous, M.; Belgacem, M. N.; Branciforti, M. C.; Bretas, R. E. S.; Bras, J. *Ind. Crops Prod.* **2015**, *70*, 134.
8. España, J. M.; Fages, E.; Moriana, R.; Boronat, T.; Balart, R. *Polym. Compos.* **2012**, *33*, 1288.
9. Fu, X.; Shen, Y.; Jiang, X.; Huang, D.; Yan, Y. *Carbohydr. Polym.* **2011**, *85*, 221.
10. Pang, H. T.; Chen, X. G.; Park, H. J.; Cha, D. S.; Kennedy, J. F. *Carbohydr. Polym.* **2007**, *69*, 419.
11. Badawy, M. E. I.; Rabea, E. I.; Rogge, T. M.; Stevens, C. V.; Smagghe, G.; Steurbaut, W.; Höfte, M. *Biomacromolecules* **2004**, *5*, 589.
12. Ali, S. W.; Rajendran, S.; Joshi, M. *Carbohydr. Polym.* **2011**, *83*, 438.
13. Pan, A. W.; Wu, B. B.; Wu, J. M. *Chin. Chem. Lett.* **2009**, *20*, 79.
14. Cerkez, I.; Kocer, H. B.; Worley, S. D.; Broughton, R. M.; Huang, T. S. *React. Funct. Polym.* **2012**, *72*, 673.
15. Chen, Y.; Han, Q. *Appl. Surf. Sci.* **2011**, *257*, 6034.
16. Williams, D. E.; Elder, E. D.; Worley, S. D. *Appl. Environ. Microbiol.* **1988**, *54*, 2583.
17. Dong, A.; Zhang, Q.; Wang, T.; Wang, W.; Liu, F.; Gao, G. *J. Phys. Chem. C* **2010**, *114*, 17298.
18. Cheng, X.; Ma, K.; Li, R.; Ren, X.; Huang, T. S. *Appl. Surf. Sci.* **2014**, *309*, 138.
19. Ali, S. W.; Joshi, M.; Rajendran, S. *Adv. Sci. Lett.* **2010**, *3*, 452.

20. Magdalena, GD. y s.; Jadwiga, O. C. *Colloids Surf. B* **2011**, *16*, 15.
21. Swapna Joseph, C.; Harish Prashanth, K. V.; Rastogi, N. K.; Indiramma, A. R.; Yella Reddy, S.; Raghavarao, K. S. M. S. *Food Bioprocess Technol.* **2011**, *4*, 1179.
22. Fajardo, A. R.; Lopes, L. C.; Rubira, A. F.; Muniz, E. C. *Chem. Eng. J.* **2012**, *183*, 253.
23. Li, H.; Gao, X.; Wang, Y.; Zhang, X.; Tong, Z. *Int. J. Biol. Macromol.* **2013**, *52*, 275.
24. Puišo, J.; Prosyčevas, I.; Guobienė, A.; Tamulevičius, S. *Mat. Sci. Eng. B* **2008**, *149*, 230.
25. Bin Ahmad, M.; Lim, J. J.; Shameli, K.; Ibrahim, N. A.; Tay, M. Y. *Molecules* **2011**, *16*, 7237.
26. Zhu, M.; He, B.; Shi, W.; Feng, Y.; Ding, J.; Li, J.; Zeng, F. *Fuel* **2010**, *89*, 2299.
27. Pereira, V. A., Jr.; de Arruda, I. N. Q.; Stefani, R. *Food Hydrocoll.* **2015**, *43*, 180.
28. Lewandowska, K. *Thermochim. Acta* **2009**, *493*, 42.
29. Abdelrazek, E. M.; Elashmawi, I. S.; Labeeb, S. *Phys. B* **2010**, *405*, 2021.
30. Li, R.; Hu, P.; Ren, X.; Worley, S. D.; Huang, T. S. *Carbohydr. Polym* **2013**, *92*, 534.